

Submicrosecond electro-optical switching of one-dimensional soft photonic crystals

LINGLING MA,^{1,2,3}  CHAOYI LI,^{2,3} LUYAO SUN,¹ ZHENPENG SONG,¹ YANQING LU,^{2,3,4} AND BINGXIANG LI^{1,2,5} 

¹College of Electronic and Optical Engineering and College of Microelectronics, Nanjing University of Posts and Telecommunications, Nanjing 210023, China

²National Laboratory of Solid State Microstructures, Nanjing University, Nanjing 210093, China

³Collaborative Innovation Center of Advanced Microstructures and College of Engineering and Applied Sciences, Nanjing University, Nanjing 210093, China

⁴e-mail: yqlu@nju.edu.cn

⁵e-mail: bqli@njupt.edu.cn

Received 23 November 2021; revised 17 December 2021; accepted 11 January 2022; posted 14 January 2022 (Doc. ID 449284); published 1 March 2022

Soft photonic crystals are appealing due to their self-assembly ability, wide tunability, and multistimuli-responsiveness. However, their response time is relatively slow, ranging from milliseconds to minutes. Here, we report submicrosecond switching of chiral liquid crystals (LCs) with 1D photonic microstructures, where electric fields modify the orientational order of molecules and quench their fluctuations, rather than altering the orientation. Thus, the adjusted refractive indices result in a fast shift of the photonic bandgap, on the order of 100 ns, which is four orders of magnitude faster than conventional electro-optic switching in cholesterics. This work offers tremendous opportunities for soft photonic applications. © 2022 Chinese Laser Press

<https://doi.org/10.1364/PRJ.449284>

1. INTRODUCTION

The rapid manipulation of the flow of light in photonic microstructures has been increasingly investigated in nano-optics and nanophotonics [1–4]. Thanks to the excellent tunability, multistimuli-responsiveness, and easy fabrication [5], photonic devices based on soft self-assembly materials have gained significant attention [6,7], whereas one of the key challenges is related to the unsatisfactory response time. Liquid crystals (LCs), as excellent self-assembly building blocks, have developed many highly functional and planar optical systems, including smart windows, structured light generators, and optical communications [8–11]. To date, many efforts have been carried out in attempting to improve the response time. For instance, the simple ordered structure and proper physical anisotropies make nematic LC indefectible in display industries and other light modulation applications [12–14]. LC molecules respond to the electric field by reorienting the director, i.e., the average molecular orientation, parallel or perpendicular to the field [12,15,16]. Once the electric field is removed, the director relaxes back to the ground state with a typical response time of approximately several milliseconds [16]. Recently, nanosecond switching of nematic LC was reported, based on the electrical modification of the order parameters [17–19]. Additionally, distinct LC microstructures with different physical properties and driving schemes, such as dual-frequency LCs [20], polymer

dispersed LCs [21], and ferroelectric LCs [22], have been widely investigated to speed up operations. However, few related studies have investigated the fast switching of chiral LCs with photonic microstructures.

Chiral LCs are well known as versatile materials with Bragg reflection [23–25]. They can self-assemble into periodic helical structures with a helical pitch P comparable with the wavelengths λ of light [26,27] [Fig. 1(a)]. Thus, a strong Bragg reflection occurs, and brilliant structural colors within the photonic bandgap (PBG) are reflected, where the propagation of electromagnetic waves is forbidden. Although blue phase LC with a 3D helicity exhibits a fast response due to the multidomain morphology (tens of microseconds) [28], its instability restricts applications in next-generation nanophotonic technology. On the other hand, 1D soft photonic crystal, which is cholesteric LC (CLC) with 1D helical microstructure, is particularly fascinating due to its tunable and broad PBG, which plays a pivotal role in the development of nanocavities [29], microsensing [30], and Berry-phase optics [31]. Usually, the application of an electric field makes CLC switch between the homeotropic state and the planar state, which means that the LC molecular reorientation process is accompanied by an unwinding process [32,33], thus resulting in a slow response time. By adopting a dual-frequency CLC, an optical beam deflector with the response time reduced to 451 ms is reported

[34]. The switching from the focal conic to the planar state can be accelerated by applying an in-plane electric field (5–150 ms) [35]. Furthermore, a nanopore-embedded cholesteric liquid crystal film is proposed with a submillisecond response [36]. Nevertheless, it is still necessary and challenging to achieve fast electro-optic switching of soft photonic crystals.

Here, we demonstrate the fast electro-optic switching of CLCs composed of a negative nematic host and a chiral dopant. The location of the PBG is optimized by tuning the concentration c of the chiral dopant, to match the probe laser beam. An electric field is applied to shift the PBG by modifying the orientational order of LC molecules and quenching the director fluctuations rather than unwinding the helical structure. Consequently, the light transmittance is rapidly modulated with a response time of 100 ns, which is the fastest electro-optic response obtained in CLCs, to the best of our knowledge. This work provides new opportunities for chiral LCs in advanced photonic applications, such as lasing, optical memories, data processing, optical computers, and multiplexing techniques.

2. RESULTS AND DISCUSSIONS

The CLC mixtures are composed of a host nematic LC with a negative dielectric anisotropy and a guest chiral dopant. When mixtures are infiltrated into a unidirectionally aligned cell, a self-assembled 1D helical structure with planar texture is formed [Figs. 1(a) and 1(b)]. Here, we define the alignment direction as the x axis and the helical axis as the z axis. The director distribution can be expressed as $n_x = \cos(qz)$, $n_y = \sin(qz)$, and $n_z = 0$, where $q = 2\pi/P$ and the CLC pitch P is defined as the distance over which the director twists by 2π . Usually, P is determined by $P = 1/(\text{HTP} \cdot c)$, where HTP and c are the helical twisting power and the mass fraction of the guest chiral agent, respectively. The period of the helical structure is $P/2$ due to the pseudovector characteristic of the LC director, i.e., $\hat{\mathbf{n}} = -\hat{\mathbf{n}}$. Thanks to the periodically modulated optical tensor, a PBG is created in CLC, of which the center is $\lambda_c = (\lambda_1 + \lambda_2)/2$, where

$$\lambda_1 = n_o P, \tag{1}$$

$$\lambda_2 = n_e P, \tag{2}$$

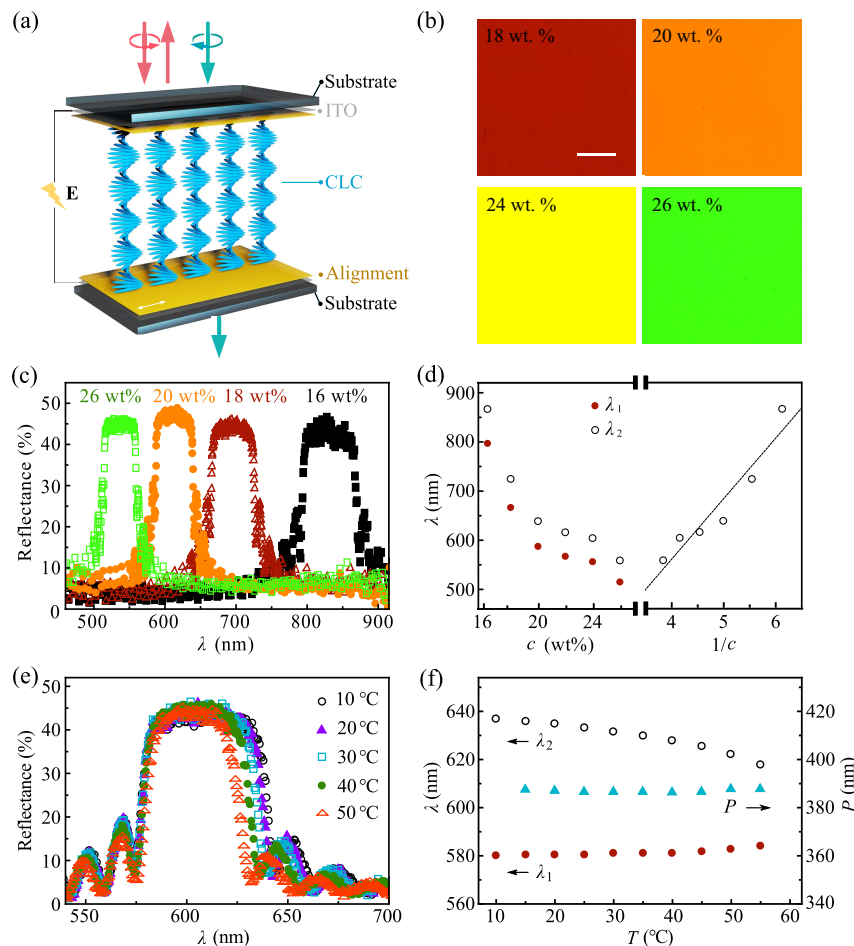


Fig. 1. Optical characteristics of CLCs. (a) Schematic illustration of the 1D helical structure. Blue rods represent LC directors. White bidirectional arrow denotes the alignment direction. Green and pink arrows indicate the transmission and reflection of light. (b) POM images of planar CLCs at different c . They are taken under the reflection mode. Scale bar, 200 μm . (c) Reflection spectra of CLC mixtures with different c . The incident laser beam is linearly polarized. (d) Dependencies of λ_1 and λ_2 on c and $1/c$. The dashed line is a linear fitting. (e) Reflection spectra of the CLC mixture at different temperatures. (f) λ_1 , λ_2 , and P as functions of the temperature at $c = 20.6\%$.

where n_o and n_e represent the ordinary and extraordinary refractive indices of LCs, respectively. λ_1 and λ_2 ($\lambda_1 < \lambda_2$) represent wavelengths at two edges of the PBG [16], referring to the locations that are with 80% of the maximum reflected intensity.

The PBG of CLC can be tuned by changing c and HTP of the guest chiral dopant or n_e and n_o of the host LC. Here, one of the PBG edges is optimized by altering c , to satisfy the wavelength of the probe laser (632.8 nm). Several CLC mixtures with different c (16%, 18%, 20%, 22%, 24%, and 26%) are prepared at 24°C with a cell thickness of 6.2 μm . As shown in Figs. 1(c) and 1(d), the PBG shows a blueshift (λ_1 decreases from 800 nm to 520 nm and λ_2 decreases from 870 nm to 560 nm) as c increases from 16% to 26%, which is consistent with $\lambda = n/(\text{HTP} \cdot c)$. The above results suggest that the HTP of S811 is approximately 11.7 μm^{-1} . Thus, to obtain $\lambda_2 \approx 632.8$ nm, c is calculated as 20.6%.

The temperature-dependencies of parameters λ_1 , λ_2 , and P are further investigated with the CLC mixture of $c = 20.6\%$. As the temperature rises from 10°C to 50°C, λ_1 does not change much, while λ_2 reduces from 639 nm to 615 nm [Figs. 1(e) and 1(f)]. Then, the variation in P is also measured by adopting the Grandjean–Cano wedge method [16]. As presented in Fig. 1(f), P is about 387 nm, nearly independent of the temperature. Thus, according to Eqs. (1) and (2), the shift of λ_2 is attributed to the decrease of n_e , which results from the temperature-induced reduction of the orientational order of CLCs. Therefore, we have reason to believe that, in addition to P , another dimension, i.e., the orientational order, can tune the PBG as well, without destroying the photonic nanostructure.

To explore the fast electro-optic responses of CLC, we use a left-handed circularly polarized laser beam ($\lambda = 632.8$ nm) normally incident to the cell at 50°C. Then, short DC voltage pulses with varied amplitudes of electric field E are applied to the sample along the helical axis. The duration is 650 ns. Due to the negative dielectric anisotropy, the electric field does not reorient LC directors but increases the arrangement order of CLC. As a result, the modulation depth of the transmitted light intensity ΔI monotonously increases with the growth of E [Figs. 2(a) and 2(b)]. When $E_5 \approx 142$ V/ μm , ΔI reaches $\sim 40\%$. From a practical point of view, we use the industry-standard 10-to-90 switching time to characterize the response of CLCs, where the response time τ is calculated as the intensity changes from 10% to 90% of the maximum change of the transmitted light intensity ΔI_{max} during the switch-on process (τ_{on}) and from 90% to 10% of ΔI_{max} during the switch-off process (τ_{off}). The maximum response time $\tau_{\text{max}} = \text{Max}[\tau_{\text{on}}, \tau_{\text{off}}]$ continuously decreases from ~ 300 ns to ~ 110 ns as E increases from ~ 32 V/ μm to ~ 142 V/ μm , as shown in Fig. 2(c), which is four orders of magnitude faster than the conventional electro-optic responses of CLCs.

To further examine the mechanism of the submicrosecond response of soft photonic crystal materials, we investigate related electric effects during the switching process. Due to the complexity of CLC with continuously varied director orientations along the helical axis, LC molecules, which are arranged in a quasi-nematic manner (Fig. 3), within a localized layer are extracted to provide a clearer picture of the optical tensor modification. In the absence of the electric field, LC molecules show a uniaxial orientational order with the optical tensor $n_x > n_y = n_z$ [Fig. 3(a)]. Due to the thermodynamic effect,

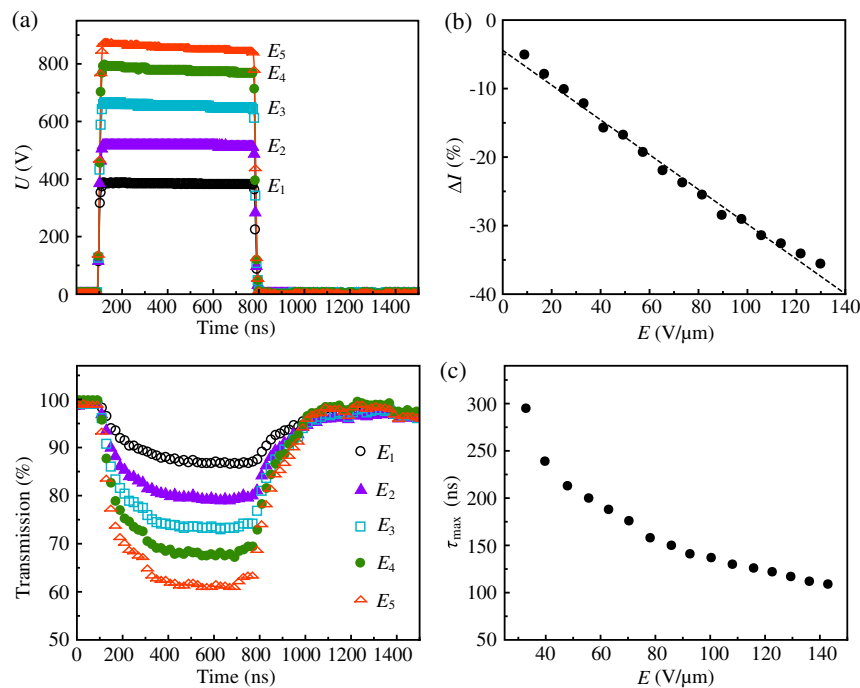


Fig. 2. Electro-optic responses of CLC. (a) Dynamics of the transmitted light intensity of CLC under $E_1 \approx 62$ V/ μm , $E_2 \approx 84$ V/ μm , $E_3 \approx 107$ V/ μm , $E_4 \approx 128$ V/ μm , and $E_5 \approx 142$ V/ μm . (b) ΔI as a function of E . The dashed line shows the linear fitting. (c) Dependency of τ_{max} on E .

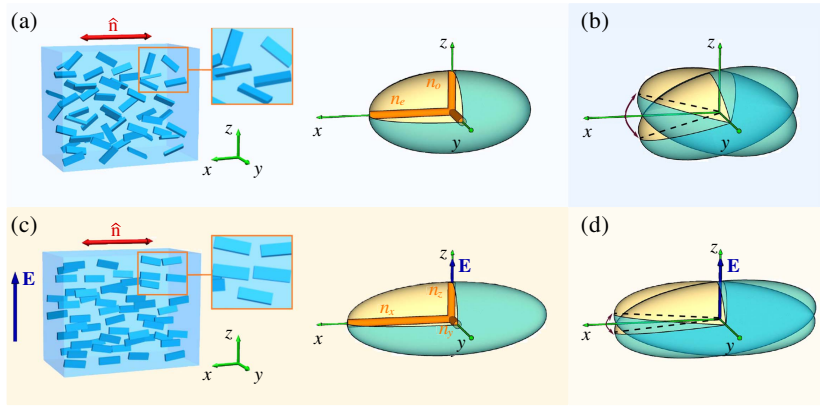


Fig. 3. Schematic illustration of field-induced effects. (a) Orientational order of LC molecules and ellipsoid optical tensor in the absence of an electric field. (b) Thermal fluctuation of the optical tensor. (c) Orientational order of LC molecules and elongated oblate optical tensor under an electric field. (d) Quenching of the optical tensor fluctuation.

thermal fluctuations exist, which will reduce the birefringence of LCs [Fig. 3(b)]. After an electric field is applied, three effects are induced, while the orientations of LC molecules with D_{2h} symmetry (like a book) are retained [17–19]. First, the uniaxial order of the long axes of LC molecules is enhanced. Second, another orientational order, i.e., the short axis, is caused, which leads to a biaxial optical tensor with $n_x > n_z > n_y$ [Fig. 3(c)]. Moreover, the director fluctuation is quenched by the electric field, which also improves the long-axis optical anisotropy [Fig. 3(d)].

To distinguish the main contribution to the fast switching of CLC, we utilize three experimental geometries [18] (see the Materials and Methods section). In geometry BU, the field-induced effective birefringence change δn is caused by the biaxial and uniaxial contributions [Fig. 4(a)]. This geometry is related to the modification of biaxial and uniaxial order parameters, also called the electric modification of order parameter (EMOP) effect [17,19]. In geometry UF, the δn is caused by the uniaxial and fluctuation contributions [Fig. 4(b)]. In geometry FBU, the laser beam is normally incident to the CLC cell; thus, all three contributions have effects on the optical response [Fig. 4(c)].

Then, we investigate the corresponding field-induced birefringence change. Detailed experimental methods are described in the Materials and Methods section. As a result, the δn in geometry BU is much larger than that in geometries UF and FBU at $E_5 \approx 142 \text{ V}/\mu\text{m}$ [Fig. 5(a)], indicating that the main contributions come from the field-induced biaxial order parameter and the enhanced uniaxial order parameters. The quenching of the director fluctuation has a relatively small contribution to the fast response. Considering the real scenario of CLC, the exclusion of the quenching of the director fluctuation in geometry BU is impractical. Therefore, the δn and response time of the nematic LC host are examined in detail in geometry FBU. The δn changes under different E are presented in Fig. 5(b). An extraordinary refractive index change $\delta n_e \approx 8 \times 10^{-3}$ is achieved at $E_5 \approx 142 \text{ V}/\mu\text{m}$, which is in good agreement with the shift of PBG about 3 nm, according to $\Delta\lambda_2 = \delta n_e P$. Additionally, the dependency of the maximum birefringence change δn_{max} on E is analyzed. With small

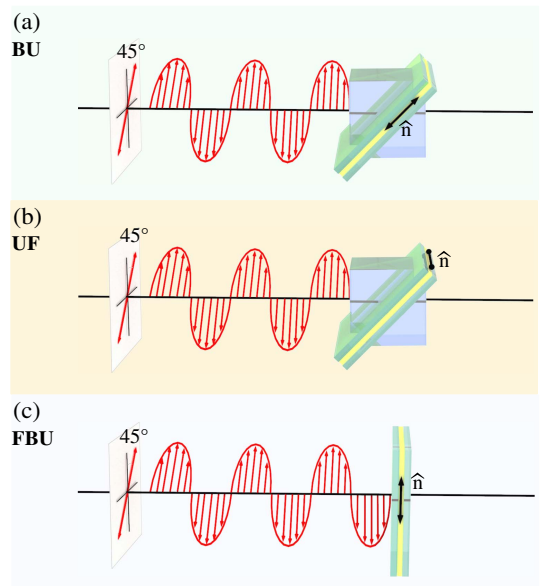


Fig. 4. Three experimental geometries. (a) Geometry BU: \hat{n} orients parallel to the plane of incidence. (b) Geometry UF: \hat{n} is perpendicular to the plane of incidence. (c) Geometry FBU: the laser beam is normally incident to the cell. The polarization is 45° with respect to \hat{n} . Red bidirectional arrows indicate the incident polarizations. Black bidirectional arrows represent the alignment of LCs. In both BU and UF geometries, the incident angles are 45° , and the polarization of the incident light is 45° with respect to the plane of incidence.

amplitudes of the electric field, δn_{max} grows proportionally to E^2 (dashed line) [Fig. 5(c)]. After E is larger than $80 \text{ V}/\mu\text{m}$, δn_{max} becomes slower than the square of the applied field. Figure 5(d) exhibits the relationship between the characteristic τ_{max} and E . As the electric field increases from $40 \text{ V}/\mu\text{m}$ to $170 \text{ V}/\mu\text{m}$, τ_{max} shows a decreasing trend from $\sim 280 \text{ ns}$ to $\sim 100 \text{ ns}$ [Fig. 5(d)], which is consistent with the response time measured in CLC. The above results provide supporting evidence for the intrinsic mechanism of submicrosecond

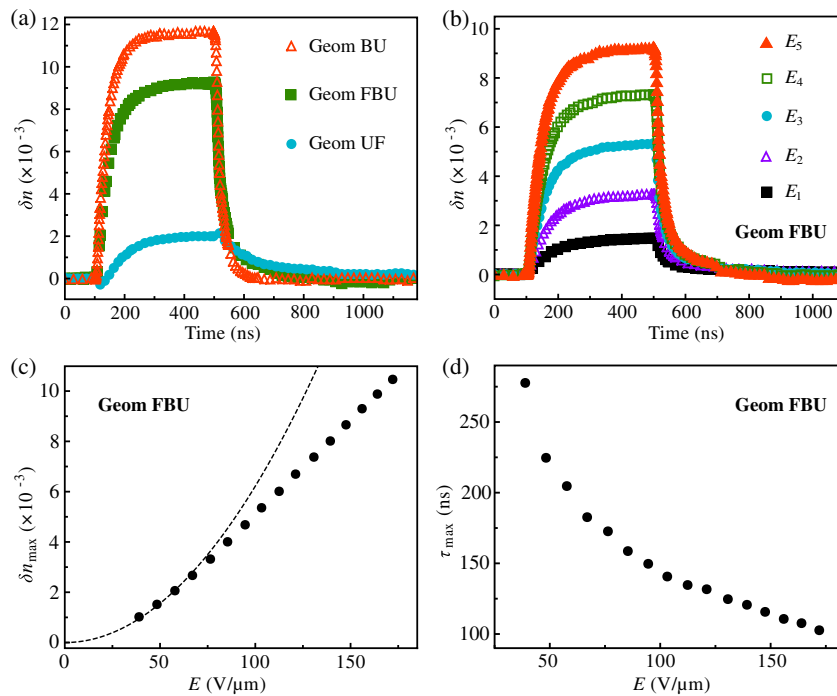


Fig. 5. Submicrosecond electro-optic switching of the nematic LC host. (a) Field-induced δn in three geometries. The duration of DC pulse is 400 ns; the amplitude is $142 \text{ V}/\mu\text{m}$. (b) Dynamics of δn at different E . (c) Dependency of δn_{\max} on E . The dashed line is a parabola fitted curve. (d) Dependence of the τ_{\max} on the E . Data in (b)–(d) are obtained from experiments in geometry FBU.

electro-optic switching of CLC, that is the field-induced swift change of the refractive indices, then the shift of PBG, and consequently, the modulation of the light transmittance.

3. CONCLUSIONS

In conclusion, we demonstrate submicrosecond electro-optic switching of a soft chiral photonic crystal material that is composed of a negative nematic LC host and a chiral dopant. The addition of the chiral dopant triggers the self-assembly of a helical configuration, where the chirality is transferred from the molecular nanoscale to the structural microscale. The concentration of chiral dopant is optimized so that one of the PBG edges matches the wavelength of the probe laser beam. Due to the negative dielectric anisotropy of the LC host, the vertical electric field does not reorient the LC directors but modifies the orientational order parameter of LC molecules. Distinct from the switching principle in nematic LCs [17–19], the refractive index change of CLCs causes the shift of PBG, which alters the forbidden state of photons and, consequently, causes the modulation of light transmittance. The electro-optic response of CLCs is also compared with that of the nematic LC host, which presents a close response time under the same E in geometry FBU. In this case, both the EMOP and the quenching of the director fluctuations have effects on the submicrosecond switching of CLCs. Hence, the response time of CLCs for modulating the transmitted light intensity is fast, on the time scale of 100 ns, which is at least four orders of magnitude faster than conventional electro-optic switching of CLCs. Moreover, the response time could be further accelerated by adopting a nematic LC material with low viscosity.

The field-induced refractive index change is approximately 0.01, which leads to a small shift of PBG around the wavelength of 632.8 nm. Fortunately, by adopting nematic hosts with larger birefringence, the edge shift of PBG can be substantially increased, thus enhancing the light modulation. By doping a photoresponsive additive into CLCs, the position of PBG can be modulated by union control of light exposure and electric field [37–39]. Thus, the range of the working wavelength can be largely extended. The fast switching of CLCs is based on the shift of PBG with a circular polarization selectivity, which allows unique highly functional photonic devices beyond the modulation of the optical phase retardation. In addition, one can devise many more ways of manipulating the flow of light by suitably combining the rapid switching mechanism of CLCs with special optical elements, such as polarization gratings, microlasers, Pancharatnam–Berry lenses, metasurfaces, and fibers.

4. MATERIALS AND METHODS

Materials: CLC mixtures were composed of a nematic LC host HNG715600-100 (Jiangsu Hecheng Display Technology) and the guest chiral dopant S811, (S)-2-octyl 4-[4-(hexyloxy)benzoyloxy]benzoate (Merck KGaA) with various concentrations. The dielectric anisotropy of HNG715600-100 is -12.2 at $T = 25^\circ\text{C}$ and $f = 1 \text{ kHz}$. $n_e = 1.646$ and $n_o = 1.493$ at $T = 20^\circ\text{C}$ and $\lambda = 589 \text{ nm}$. All the mixtures were kept in the isotropic phase for 10 h and vortexed for 3 min before being filled into cells.

Sample fabrication: Glass substrates ($10 \text{ mm} \times 10 \text{ mm}$) were coated with indium tin oxide (low resistivity, $10 \Omega/\text{sq}$)

with the active area of electrodes 2 mm × 2 mm. The substrates were ultrasonically bathed, and UV-ozone cleaned. Then, polyimide PI-2555 (HD Microsystems) was spin-coated onto substrates and unidirectionally rubbed to induce planar (homogeneous) alignments. Two pieces of glass substrates were separated by 6.2 μm spacers and sealed with epoxy glue to fabricate an LC cell. The CLC mixtures were capillary-filled into planar cells in the isotropic phase and slowly cooled to the cholesteric phase at the rate of 1°C/min.

Characterizations: The reflection spectra of CLCs were measured with unpolarized light (Tungsten halogen lamp LS-1, Ocean Optics), a polarizer, a spectrometer (USB4000 UV-VIS, Ocean Optics), and a hot stage (PE94, Linkam). The nanosecond DC voltage pulses were generated by a pulse generator (HV 1000, Direct Energy) with sharp rise and fall edges with the characteristic time of 1 ns. A circularly polarized laser beam was generated by a He–Ne laser ($\lambda = 632.8$ nm), linear polarizer, and quarter-wave plate. The transmitted intensity of the circularly polarized light was measured by a photodetector (TIA-525, Terahertz Technologies). We used a digital oscilloscope (TDS2014, 1 GSa/s, Tektronix) to record voltages and photodetector signals. To characterize the field-induced effective birefringence change of the nematic LC host, we used the experimental setup described in Refs. [13,14], where a He–Ne laser beam passed through a polarizer, an LC cell, an adjustable optic compensator, and another polarizer crossed with the first one. The transmitted light intensity was measured with two settings of the compensator (noted as A and B), where the phase retardance difference is $\Gamma_B - \Gamma_A = \pi$. In the absence of an electric field, the measured intensities of the transmitted light from these settings are $I_A(0) = I_B(0) = (I_{\max} + I_{\min})/2$, where I_{\max} and I_{\min} are the maximum and minimum transmitted intensities determined by adjusting the optical retardance of the compensator. The dynamics of the $\delta n(t)$ is determined by the field-induced phase retardance $\delta\Gamma$ as [40]

$$\delta n(t) = \frac{\lambda\delta\Gamma}{2\pi d} = \frac{\lambda}{2\pi d} \arcsin \frac{I_A(t) - I_B(t)}{I_{\max} - I_{\min}}. \quad (3)$$

Experimental geometries: The δn_{BU} , δn_{UF} , and δn_{FBU} in three geometries BU, UF, and FBU (Fig. 4) are [18]

$$\delta n_{\text{BU}} = \frac{n_o/n_e + 1 + n_e/n_o}{6\sqrt{n_e^2 - n_o^2}} \left(\delta\tilde{\epsilon}_u + \frac{3}{2}\delta\tilde{\epsilon}_b \right), \quad (4)$$

$$\delta n_{\text{UF}} = \frac{1}{3\sqrt{2}} \left(\frac{1}{n_o} + \frac{2}{\sqrt{2n_e^2 - n_o^2}} \right) \left(\delta\tilde{\epsilon}_u + \frac{3}{2}\delta\tilde{\epsilon}_f \right), \quad (5)$$

and

$$\delta n_{\text{FBU}} = \frac{1}{6n_o} \left(\delta\tilde{\epsilon}_u + \frac{3}{2}\delta\tilde{\epsilon}_b \right) + \frac{1}{3n_e} \left(\delta\tilde{\epsilon}_u + \frac{3}{2}\delta\tilde{\epsilon}_f \right), \quad (6)$$

respectively. Here, $\delta\tilde{\epsilon}_u$, $\delta\tilde{\epsilon}_b$, and $\delta\tilde{\epsilon}_f$ are the electro-optic contributions from the enhanced uniaxial order parameter, the induced biaxial order parameter, and the quenching of the director fluctuations, respectively. In geometry BU, the incident angle of the laser beam is 45° with respect to the normal of the cell. The $\hat{\mathbf{n}}$ is in the plane of incidence and parallel to the substrates. In UF geometry, the incident angle is 45°. The $\hat{\mathbf{n}}$ is perpendicular to the plane of incidence. In geometry FBU, the laser beam is normal to the LC cell, and $\hat{\mathbf{n}}$ is parallel to the

substrates. The angle between the polarization of incident light and the plane of incidence is 45° in all three geometries.

Funding. National Key Research and Development Program of China (2021YFA1202000); National Natural Science Foundation of China (RK106LH21001, 52003115); Natural Science Foundation of Jiangsu Province (BK20212004, BK20200320); Innovation and Entrepreneurship Program of Jiangsu Province.

Acknowledgment. The authors gratefully appreciate Prof. Oleg D. Lavrentovich for his constructive discussions.

Disclosures. The authors declare that they have no conflicts of interest.

Data Availability. Data underlying the results presented in this paper are not publicly available at this time but may be obtained from the authors upon reasonable request.

REFERENCES

1. Y. Zhou, Z. Yuan, X. Gong, M. Birowosuto, C. Dang, and Y. C. Chen, "Dynamic photonic barcodes for molecular detection based on cavity-enhanced energy transfer," *Adv. Photon.* **2**, 066002 (2020).
2. Y. Wang, Q. Chen, W. Yang, Z. Ji, L. Jin, X. Ma, Q. Song, A. Boltasseva, J. Han, V. M. Shalae, and S. Xiao, "High-efficiency broadband achromatic metalens for near-IR biological imaging window," *Nat. Commun.* **12**, 5560 (2021).
3. J. Xiong and S. T. Wu, "Planar liquid crystal polarization optics for augmented reality and virtual reality: from fundamentals to applications," *eLight* **1**, 3 (2021).
4. Y. Xiong and F. Xu, "Multifunctional integration on optical fiber tips: challenges and opportunities," *Adv. Photon.* **2**, 064001 (2020).
5. J. Hu, W. Wang, and H. Yu, "Endowing soft photo-actuators with intelligence," *Adv. Intell. Syst.* **1**, 1900050 (2019).
6. M. Kollé and S. Lee, "Progress and opportunities in soft photonics and biologically inspired optics," *Adv. Mater.* **30**, 1702669 (2018).
7. C. Ropp, N. Bachelard, D. Barth, Y. Wang, and X. Zhang, "Dissipative self-organization in optical space," *Nat. Photonics* **12**, 739–743 (2018).
8. L. Wang, H. K. Bisoyi, Z. Zheng, K. G. Gutierrez-Cuevas, G. Singh, S. Kumar, T. J. Bunning, and Q. Li, "Stimuli-directed self-organized chiral superstructures for adaptive windows enabled by mesogen-functionalized graphene," *Mater. Today* **20**, 230–237 (2017).
9. L. Qin, W. Gu, J. Wei, and Y. Yu, "Piecewise phototuning of self-organized helical superstructures," *Adv. Mater.* **30**, 1704941 (2018).
10. Y. Liu, H. Liang, C. W. Chen, X. Xie, W. Hu, P. Chen, J. Wen, J. Zhou, T. H. Lin, and I. C. Khoo, "Ultrafast switching of optical singularity eigenstates with compact integrable liquid crystal structures," *Opt. Express* **26**, 28818–28826 (2018).
11. D. Chen, M. R. Tuchband, B. Horanyi, E. Korblova, D. M. Walba, M. A. Glaser, J. E. MacLennan, and N. A. Clark, "Diastereomeric liquid crystal domains at the mesoscale," *Nat. Commun.* **6**, 7763 (2015).
12. C. G. Pochi Yeh, *Optics of Liquid Crystal Displays* (Wiley, 1999).
13. Q. H. Wang, F. Chu, H. Dou, L. L. Tian, R. Li, and W. Y. Hou, "A single-cell-gap transmissive liquid crystal display with a vertically aligned cell," *Liq. Cryst.* **46**, 1183–1190 (2018).
14. Y. H. Lin, Y. J. Wang, H. C. Lin, M. L. Lee, and P. L. Chen, "Optical measurement in a curved optical medium with optical birefringence and anisotropic absorption," *Opt. Express* **29**, 38654–38668 (2021).
15. Z. Shen, S. Zhou, X. Li, S. Ge, P. Chen, W. Hu, and Y. Lu, "Liquid crystal integrated metalens with tunable chromatic aberration," *Adv. Photon.* **2**, 036002 (2020).
16. D. K. Yang and S. T. Wu, *Fundamentals of Liquid Crystal Devices*, 2nd ed. (Wiley, 2014).

17. V. Borshch, S. V. Shiyankovskii, and O. D. Lavrentovich, "Nanosecond electro-optic switching of a liquid crystal," *Phys. Rev. Lett.* **111**, 107802 (2013).
18. V. Borshch, S. V. Shiyankovskii, B. X. Li, and O. D. Lavrentovich, "Nanosecond electro-optics of a nematic liquid crystal with negative dielectric anisotropy," *Phys. Rev. E* **90**, 062504 (2014).
19. B. X. Li, V. Borshch, S. V. Shiyankovskii, S. B. Liu, and O. D. Lavrentovich, "Electro-optic switching of dielectrically negative nematic through nanosecond electric modification of order parameter," *Appl. Phys. Lett.* **104**, 201105 (2014).
20. Y. H. Fan, H. Ren, X. Liang, Y. H. Lin, and S. T. Wu, "Dual-frequency liquid crystal gels with submillisecond response time," *Appl. Phys. Lett.* **85**, 2451–2453 (2004).
21. S. Pagidi, R. Manda, S. S. Bhattacharyya, S. G. Lee, S. M. Song, Y. J. Lim, J. H. Lee, and S. H. Lee, "Fast switchable micro-lenticular lens arrays using highly transparent nano-polymer dispersed liquid crystals," *Adv. Mater. Interfaces* **6**, 1900841 (2019).
22. Q. Guo, K. Yan, V. Chigrinov, H. Zhao, and M. Tribelsky, "Ferroelectric liquid crystals: physics and applications," *Crystals* **9**, 470 (2019).
23. Z. G. Zheng, Y. Li, H. K. Bisoyi, L. Wang, T. J. Bunning, and Q. Li, "Three-dimensional control of the helical axis of a chiral nematic liquid crystal by light," *Nature* **531**, 352–356 (2016).
24. W. Hu, H. Zhao, L. Song, Z. Yang, H. Cao, Z. Cheng, Q. Liu, and H. Yang, "Electrically controllable selective reflection of chiral nematic liquid crystal/chiral ionic liquid composites," *Adv. Mater.* **22**, 468–472 (2010).
25. L. J. Chen, L. L. Gong, Y. L. Lin, X. Y. Jin, H. Y. Li, S. S. Li, K. J. Che, Z. P. Cai, and C. J. Yang, "Microfluidic fabrication of cholesteric liquid crystal core-shell structures toward magnetically transportable micro-lasers," *Lab Chip* **16**, 1206–1213 (2016).
26. J. Li, H. K. Bisoyi, J. Tian, J. Guo, and Q. Li, "Optically rewritable transparent liquid crystal displays enabled by light-driven chiral fluorescent molecular switches," *Adv. Mater.* **31**, 1807751 (2019).
27. J. Xiang, Y. Li, Q. Li, D. A. Paterson, J. M. D. Storey, C. T. Imrie, and O. D. Lavrentovich, "Electrically tunable selective reflection of light from ultraviolet to visible and infrared by heliconical cholesterics," *Adv. Mater.* **27**, 3014–3018 (2015).
28. Y. Li, S. Huang, P. Zhou, S. Liu, J. Lu, X. Li, and Y. Su, "Polymer-stabilized blue phase liquid crystals for photonic applications," *Adv. Mater. Technol.* **1**, 1600102 (2016).
29. H. Coles and S. Morris, "Liquid-crystal lasers," *Nat. Photonics* **4**, 676–685 (2010).
30. D. J. Mulder, A. P. H. J. Schenning, and C. W. M. Bastiaansen, "Chiral-nematic liquid crystals as one dimensional photonic materials in optical sensors," *J. Mater. Chem. C* **2**, 6695–6705 (2014).
31. P. Chen, L. L. Ma, W. Hu, Z. X. Shen, H. K. Bisoyi, S. B. Wu, S. J. Ge, Q. Li, and Y. Q. Lu, "Chirality invertible superstructure mediated active planar optics," *Nat. Commun.* **10**, 2518 (2019).
32. W. S. Li, L. L. Ma, L. L. Gong, S. S. Li, C. Yang, B. Luo, W. Hu, and L. J. Chen, "Interlaced cholesteric liquid crystal fingerprint textures via sequential UV-induced polymer-stabilization," *Opt. Mater. Express* **6**, 19–28 (2016).
33. K. H. Kim, D. H. Song, Z. G. Shen, B. W. Park, K. H. Park, J. H. Lee, and T. H. Yoon, "Fast switching of long-pitch cholesteric liquid crystal device," *Opt. Express* **19**, 10174–10179 (2011).
34. X. Shang, L. Meeus, D. Cuyppers, and H. De Smet, "Fast switching cholesteric liquid crystal optical beam deflector with polarization independence," *Sci. Rep.* **7**, 6492 (2017).
35. S. W. Oh and T. H. Yoon, "Fast bistable switching of a cholesteric liquid crystal device induced by application of an in-plane electric field," *Appl. Opt.* **53**, 7321–7324 (2014).
36. H. Yoshida, Y. Inoue, Y. Shiozaki, M. Takahashi, H. Kubo, A. Fujii, and M. Ozaki, "Fast and continuous tunable lasing from a nano-pore embedded cholesteric liquid crystal film," *Mol. Cryst. Liq. Cryst.* **560**, 101–107 (2012).
37. H. K. Bisoyi, T. J. Bunning, and Q. Li, "Stimuli-driven control of the helical axis of self-organized soft helical superstructures," *Adv. Mater.* **30**, 1706512 (2018).
38. K. G. Gutierrez-Cuevas, L. Wang, Z. G. Zheng, H. K. Bisoyi, G. Li, L. S. Tan, R. A. Vaia, and Q. Li, "Frequency-driven self-organized helical superstructures loaded with mesogen-grafted silica nanoparticles," *Angew. Chem. Int. Ed.* **55**, 13090–13094 (2016).
39. C. L. Yuan, W. Huang, Z. G. Zheng, B. Liu, H. K. Bisoyi, Y. Li, D. Shen, Y. Lu, and Q. Li, "Stimulated transformation of soft helix among helical, heliconical, and their inverse helices," *Sci. Adv.* **5**, eaax9501 (2019).
40. B. X. Li, G. Babakhanova, R. L. Xiao, V. Borshch, S. Siemianowski, S. V. Shiyankovskii, and O. D. Lavrentovich, "Microsecond electro-optic switching of nematic liquid crystals with giant dielectric anisotropy," *Phys. Rev. Appl.* **12**, 024005 (2019).